State-to-state reaction probabilities for the H + O 2 (v , j) → O + O H (v ′ , j ′) reaction on three potential energy surfaces

Marlies Hankel, Sean C. Smith, and Anthony J. H. M. Meijer

Citation: The Journal of Chemical Physics **127**, 064316 (2007); doi: 10.1063/1.2762220
View online: http://dx.doi.org/10.1063/1.2762220
View Table of Contents: http://scitation.aip.org/content/aip/journal/jcp/127/6?ver=pdfcov
Published by the AIP Publishing

State-to-state reaction probabilities for the $H+O_2(v,j)\rightarrow O+OH(v',j')$ reaction on three potential energy surfaces

Marlies Hankel[a),b)] and Sean C. Smith[c)]
Centre for Computational Molecular Science, Australian Institute for Bioengineering and Nanotechnology, The University of Queensland, QLD 4072, Australia

Anthony J. H. M. Meijer[a),d)]
Department of Chemistry, University of Sheffield, Sheffield S3 7HF, United Kingdom

(Received 15 May 2007; accepted 27 June 2007; published online 14 August 2007)

We report state-to-state and total reaction probabilities for $J=0$ and total reaction probabilities for $J=2$ and 4 for the title reaction, both for ground-state and initially rovibrationally excited reactants. The results for three different potential energy surfaces are compared and contrasted. The potential energy surfaces employed are the DMBE IV surface by Pastrana *et al.* [J. Phys. Chem. **94**, 8073 (1990)], the surface by Troe and Ushakov (TU) [J. Chem. Phys. **115**, 3621 (2001)], and the new XXZLG *ab initio* surface by Xu *et al.* [J. Chem. Phys. **122**, 244305 (2005)]. Our results show that the total reaction probabilities from both the TU and XXZLG surfaces are much smaller in magnitude for collision energies above 1.2 eV compared to the DMBE IV surface. The three surfaces also show different behavior with regards to the effect of initial state excitation. The reactivity is increased on the XXZLG and the TU surfaces and decreased on the DMBE IV surface. Vibrational and rotational product state distributions for the XXZLG and the DMBE IV surface show different behaviors for both types of distributions. Our results show that for energies above 1.25 eV the dynamics on the DMBE IV surface are not statistical. However, there is also evidence that the dynamics on the XXZLG surface are not purely statistical for energies above the onset of the first excited product vibrational state $v'=1$. The magnitude of the total reaction probability is decreased for $J>0$ for the DMBE IV and the XXZLG surfaces for ground-state reactants. However, for initially rovibrationally excited reactants, the total reaction probability does not decrease as expected for both surfaces. As a result the total cross section averaged over all Boltzmann accessible rotational states may well be larger than the cross section reported in the literature for $j=1$. © *2007 American Institute of Physics*. [DOI: 10.1063/1.2762220]

I. INTRODUCTION

The title reaction is a key reaction in combustion chemistry. It is responsible for chain branching in the oxidation of hydrogen and is the dominant molecular oxygen consuming step in both hydrogen-oxygen and methane-oxygen combustion processes.[1] The reverse reaction is also important in atmospheric chemistry including ozone destruction. It presents a big challenge for quantum scattering calculations because of its deep well and the heavy masses (only one hydrogen atom and two oxygen atoms) involved. As a consequence, several studies concerning the rate coefficients,[2–6] reaction dynamics,[7–24] and the reaction intermediate[25–33] are available in the literature.

There are several potential energy surfaces (PES) available.[2,5,34–36] The most widely used is the DMBE IV surface[34] due to Pastrana *et al.* which was published more than 15 years ago. Troe and Ushakov designed a global surface[2] (designated TU) on the basis of Harding's *ab initio* calculations along the minimum energy path of the $HO_2 \rightarrow H+O_2$ and $HO_2 \rightarrow HO+O$ dissociations.[25] The most recent surface, named XXZLG, by Xu *et al.*[5] has been developed by three-dimensional cubic spline interpolation of more than 15 000 *ab initio* points at the icMRCI+Q/aug-cc-pVQZ level of theory. An analytical fit to this surface was published recently.[37] Additionally, there is also the early Melius-Blint surface[36] and the diatomics-in-molecules surface of Kendrick and Pack[35] which have not been used in this paper.

In a recent letter[38] Lin, Guo, Hanvault, and Xie (LGHX) reported results of time-dependent and time-independent quantum mechanical calculations employing the XXZLG and the DMBE IV surfaces. The results for the two surfaces are significantly different with the results from the XXZLG surface much smaller in magnitude. This is especially true for energies above 1.2 eV where Meijer and Goldfield attributed the rise in the reaction probability to a direct mechanism.[15] While the results from both surfaces reasonably agree below 1.2 eV the increase above this energy is completely missing in the XXZLG results. In fact the total reaction probability is decreasing with increasing energy. LGHX attribute the absence of the increase in the total reaction probability at 1.2 eV to an artifact of the DMBE IV surface. In light of these findings we have performed time-

[a)]Authors to whom correspondence should be addressed.
[b)]Electronic mail: m.hankel@uq.edu.au
[c)]Electronic mail: s.smith@uq.edu.au
[d)]Electronic mail: a.meijer@sheffield.ac.uk

dependent wavepacket calculations employing the DMBE IV, TU, and XXZLG surfaces to investigate the influence of the PES on the reaction probabilities.

Several groups have reported total reaction probabilities for the title reaction for $J=0$. Pack *et al.*[8] reported total and cumulative reaction probabilities for the DMBE IV surface using a time-independent method. They present total reaction probabilities for the $O_2(v,j)$ ground state (0,1) and (3,1) and (0,29) in the energy range from 0.8 to 1.42 eV. The total reaction probabilities from the excited initial states are smaller in magnitude than the one from the ground state. Zhang and Zhang[9] reported total reaction probabilities for the DMBE IV surface employing a time-dependent wavepacket method. The authors reported total reaction probabilities for four different initial vibrational states of $O_2(v,j)$, (0,1), (1,1), (2,1), and (3,1). The results show that the reactivity is decreased with initial vibrational state excitation in the energy range of 0.8–1.4 eV.

Pack *et al.*[10] were the first to report state-to-state reaction probabilities for the DMBE IV surface for $J=0$. They report reaction probabilities for several excited initial rotational states summed over all final states. They also report reaction probabilities from the ground initial state to different product vibrational and rotational states. They found that initial rotational excitation has no significant effect on the reactivity in the energy range from 0.8 to 1.4 eV, only for j above 20 is the magnitude significantly decreased. The authors also conclude that the products are produced in high rotational states. This has been confirmed in 1996 by Dai and Zhang[12] who used a time-dependent wavepacket method to calculate state-to-state reaction probabilities. They report reaction probabilities for a range of product rotational states and rotational distributions from the reactant ground state for energies in the range from 0.8 to 1.5 eV. The reported rotational state distributions also show that the products are preferably produced in high rotational states.

A few years ago Sultanov and Balakrishnan[22] reported cumulative reaction probabilities for the DMBE IV and the TU surfaces employing the ABC (Ref. 39) reactive scattering program. The authors found that the cumulative reaction probability is larger for the TU surface than for the DMBE IV surface for energies between 0.8 and 1.4 eV. These calculations did include $J>0$ effects, albeit via the J-shifting approximation. It must be noted here that this approximation was shown to be inappropriate for the calculation of total reaction probabilities for this reaction due to the floppiness of the HO_2 intermediate in Ref. 18. However, this effect may be less important for the cumulative reaction probabilities due to the larger amount of averaging.

Meijer and Goldfield were the first to carry out a series of rigorous calculations for total angular momentum $J>0$.[15–18] They report total reaction probabilities from the ground state for total angular momentum quantum numbers $J=0$, 1, 2, 5, 10, 15, 20, 25, and 35 for an energy range from 0.8 to 1.8 eV. They found that for higher angular momentum quantum numbers the magnitude of the total reaction probability is significantly reduced. However, this effect is more than compensated for by the $(2J+1)$ prefactor for each reaction probability in the calculation of cross sections. As a result, the reaction probabilities for $J=10-20$ were found to have the largest contribution to the total integral cross section.[17] The resulting cross section are approximately half the experimental value. However, the energy dependence agrees well with the experimental results.[19]

In a recent study Lin *et al.*[38] report state-to-state reaction probabilities for the DMBE IV and the XXZLG surfaces employing a time-dependent wavepacket method and a time-independent method. They report reaction probabilities for three selected product rotational states from the ground reactant state for energies in the range from 0.65 to 1.6 eV for both surfaces for $J=0$. Total reaction probabilities for $O_2(v,j)=(0,3)$ and (1,1) for an energy range from 0.4 to 1.3 eV for both surfaces are also presented. From Fig. 3 in Ref. 38 it seems that the probability from (0,3) is slightly decreased for both surfaces and that initial vibrational excitation has no significant effect, again for both surfaces, for the energy range considered.

A few months ago Bargueño *et al.*[24] published a study of the title reaction using a time-dependent method and statistical methods and presented state-to-state reaction probabilities from the reactant ground state, total reaction probabilities for angular momenta $J=0$, 1, 2, 5, 10, and 15 and integral cross sections employing the DMBE IV surface. The authors report that products are formed in high rotational states, confirming the findings from the earlier calculations on the DMBE IV surface. They also conclude that the dynamics are not statistical especially above 1.2 eV. Results are reported for energies between 0.8 and 1.4 eV.

From the literature, it is clear that most of the state-to-state reaction probabilities reported to date have been for the DMBE IV surface and only in the energy range from 0.8 to 1.4 eV and for $J=0$ only. In the present study we will present total and state-to-state reaction probabilities for the DMBE IV, XXZLG, and the TU surfaces for an energy range from 0.8 to 1.8 eV. We will also investigate the effect of initial state excitation for the DMBE IV and XXZLG surfaces for $J=0$ as well as for selected $J>0$. In the latter case, we will primarily focus on initial rotational excitation, since one expects significant rotational excitation at room temperature in an experiment as performed in Ref. 19. In fact, at room temperature $O_2(v,j)=(0,9)$ and (0,11) can be expected to be populated most. In this paper we will focus on $O_2(v,j)=(0,1)$, (0,3) and (0,5) for $J>0$ to get an idea of the relevance of rotational excitation. At a later stage we intend to look at (computationally significantly more demanding) higher initial rotational excitation as well.

Section II outlines the methods employed in this study and the parameters used. Our results will be given in Sec. III which is divided into two subsections. We will first discuss the results for $J=0$. Initially, we will focus on reaction probabilities and product state distributions from the ground state. Then in Sec. III A 2 we will investigate the effect of the initial vibrational and rotational excitation on the dynamics for all three surfaces for $J=0$. Finally, in Sec. III B we will present our results for $J>0$ for the DMBE IV and the XXZLG surfaces. Finally, Sec. IV will present our conclusions.

TABLE I. Grid and initial condition details for the RWP1 and RWP2 calculations employing the DMBE IV, XXZLG, and TU surfaces. All quantities in atomic units unless stated otherwise.

Variable	RWP1	RWP2
Scattering coordinate (R) range	0.2–14.0	0.1–20.1
Number of grid points in R	229	350
Internal coordinate (r) range	0.5–17.0	0.1–20.1
Number of grid points in r	342	350
Number of angular grid points	150	56
Absorption region length in R (r)	3.5 (7.5)	3.0 (3.0)
Absorption strength in R (r)	0.414 (0.069)	0.01 (0.01)
Centre of initial wavepacket (R_0)	8.5	7.0
Width of the wavepacket α	7.0	5.56
Smoothing of the wavepacket, β	0.5	n/a
Initial translational energy (eV)	1.5	1.09
Cutoff energy V_{cut}	0.22	0.45

II. METHODS AND CALCULATION DETAILS

We denote product or final state quantum numbers with a prime, v', j', and Ω'. Quantum numbers without a prime, v, j, and Ω, denote initial state quantum numbers.

A. General comments

Two different computer programs were used in our calculations, RWP1 and RWP2. RWP1 uses the real wavepacket approach by Gray and Balint-Kurti[40] in product coordinates to be able to obtain state-to-state reaction probabilities. In RWP1 the application of the kinetic energy onto the wavepacket is done using a discrete variable representation (DVR) based on Gauss-Legendre quadrature points for the angular part and the radial kinetic energy terms are evaluated using fast Fourier transforms.[40–42] The analysis is done using the asymptotic matching method by Balint-Kurti and co-workers[40,43] This code is $J=0$ only. RWP2 also uses the real wavepacket approach, but in reactant coordinates. Moreover, a wrapped sinc-DVR (Ref. 44) is used for the application of the kinetic energy operator. In addition, a point selection scheme is used to speed up the calculations.[15] The analysis in RWP2 is done using a flux analysis method.[9] This code deals with $J\geqslant 0$. Both methods employed are well documented in the literature. For more details, see, for example, Refs. 15–17 and 40–42. The present work focuses on the effect of initial state excitation on total reaction probabilities and therefore we did not calculate state-to-state probabilities for $J>0$. However, we should mention in the context that parallel methods to calculate state-to-state properties and which are based on real wavepackets, similar in spirit to our methods, have been reported by Althorpe,[45] Yuan *et al.*,[46] Lin and Guo,[47] and our own group.[48]

B. $J=0$ calculations

All parameters used in the RWP1 and RWP2 calculations are listed in Table I. The absorption strength and length for the product and reactant channels used in the RWP1 calculations have been calculated for each channel separately. Translational energies of around 0.1 eV for reactants and around 0.6 eV for products as well as the appropriate reduced masses have been used to calculate absorption length and strength according to Refs. 49 and 50. We used the earlier reaction probabilities by Zhang and Zhang[9] and by Pack *et al.*[10] as a first reference to determine the grid density for our calculations. We performed several calculations using very small and less dense and also very large and dense grids. The grid sizes used here are those that showed the best agreement with earlier results and showed no noticeable difference in the reaction probabilities after increasing the grid size again. Please note that these earlier calculations by Zhang and Zhang were also reproduced by González-Lezana *et al.*[23]

In all RWP1 calculations the wavepacket has been propagated for 50 000 steps. Test calculations employing the DMBE IV surface for longer propagation times, up to 100 000 iteration steps, showed no significant changes in the reaction probabilities even for the low energy region. This shows that most of the resonance structures are converged after 50 000 iterations using the RWP1 approach. This holds true as well for the RWP2 calculations, which were all propagated to 60 000 steps (approximately 11 3000 a.u.). For RWP2 the calculations on the DMBE IV surface were propagated to 100 000 steps without any significant changes compared to propagating to 60 000 steps.

C. $J>0$ calculations

For the $J>0$ calculations we used most parameters from the $J=0$ calculations without change. However, we only propagated the wavepacket to 35 000 a.u. Selected initial states were propagated to 60 000 a.u. However, this only resulted in sharper resonances. No qualitative differences were found.

We performed calculations for $J=2$ and $J=4$ for initial O_2 rotational angular momentum $j=1,3,5$. In these calculations Coriolis coupling was included rigorously. All calculations were performed using the Coriolis-coupled algorithm[51] on parallel computers. All possible initial states were taken into account. The total reaction probability $P_{vj}^{J}(E)$ for initial O_2 rovibrational state (v,j) and total J at total energy E is defined as

$$P_{vj}^{J}(E)=\frac{1}{2\,\min(j,J)+1}\sum_{\Omega,p}P_{vj\Omega}^{Jp}(E), \tag{1}$$

where p is the spectroscopic parity of the wave function[52] and Ω is the projection quantum number of both j and J onto the z axis of the system, which was taken to be the scattering distance R.[16,53,54] As a result, we had to perform $\min(j,J)$ calculations of odd spectroscopic parity and $\min(j,J)+1$ calculations of even spectroscopic parity for each (j,J) combination. See Refs. 15–17 and references therein for a more extensive discussion of the theory involved and its implementation.

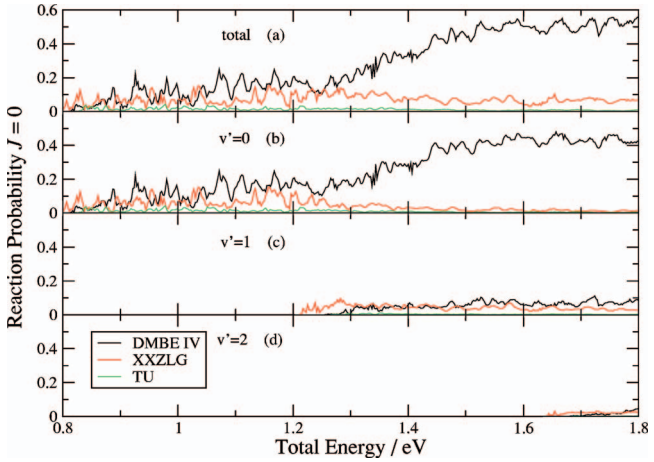

FIG. 1. (Color) State-to-state reaction probabilities vs total energy in eV obtained by the RWP1 method on the DMBE IV (black line), the XXZLG (red line), and the TU surface (green line). The total reaction probabilities and state-to-state reaction probabilities for $v'=0,1,2$ are shown.

III. RESULTS AND DISCUSSION

A. $J=0$ results

1. Total and state-to-state reaction probabilities for ground state reactants

All results in this section are for the ground state of the reactant molecule, $O_2(v=0,j=1)$.

Figure 1 shows the state-to-state reaction probabilities obtained on the DMBE IV surface, the XXZLG surface, and the TU surface employing the RWP1 method. We also calculated total reaction probabilities for all three surfaces employing the RWP2 method to check internal consistency, see Figs. 10 and 11 in the supplementary material.[55] We compared the reaction probabilities from both methods with the earlier calculations on the DMBE IV potential energy surface by Zhang and Zhang[9] and by Pack *et al.*,[10] see Fig. 10, to check the convergence of the calculations from the RWP1 and RWP2 methods.

Panel (a) of Fig. 1 shows the total reaction probabilities for all three surfaces. The probability for the DMBE IV surface is largest in magnitude and there is a significant rise in magnitude for energies above 1.2 eV. The reaction probabilities for the XXZLG surface are much smaller than the ones that have been obtained on the DMBE IV surface. For energies below 1.2 eV the probability is increasing with energy, whereas above 1.2 eV it is overall decreasing with energy. These significant differences in the reaction probabilities for the DMBE IV and XXZLG surfaces above 1.25 eV have also been observed by Lin *et al.*[38] Our results confirm these earlier results obtained by a time-dependent method, similar to ours, and by a time-independent method. It is clear to see that the probability from the TU surface is very small compared to the other two especially for higher energies. Again, also here the overall decrease of the reaction probabilities with increasing energy above 1.2 eV is clearly visible. For both the XXZLG and TU surfaces the structures above 1.2 eV are less narrow than the structures below 1.2 eV. These overall features of the resonances are similar to those found for the DMBE IV surface. Panel (b) shows the reaction probability for the OH product vibrational state $v'=0$. One can see that the DMBE IV curve still displays the increase in amplitude at around 1.25 eV which has been attributed to the onset of the direct mechanism. The curve from the XXZLG surface starts to decrease rapidly in magnitude at around 1.25 eV and goes nearly to zero for energies close to 1.8 eV. The probability also shows nearly no structure above 1.25 eV. Again the probability for the TU surface is very small but one can notice the same behavior as for the XXZLG surface, the rapid decrease for energies above 1.25 eV. Panel (c) shows the reaction probabilities for $v'=1$. The general picture here is different to the one for the ground product vibrational state. The probabilities for the DMBE IV and the XXZLG surfaces are similar in magnitude. The probability from the TU surface is hardly noticeable on the scale shown. Finally, panel (d) shows a similar picture for $v'=2$ to panel (c) for $v'=1$ with the results for the DMBE IV and the XXZLG surfaces similar in magnitude.

The differences between the reaction probabilities from the three surfaces seem to be mainly due to the differences for the ground vibrational product state. The probability for the DMBE IV surface shows a clear increase for energies above 1.25 eV while the probability for the XXZLG surface shows a clear decrease. This decrease coincides with the onset of the next vibrational product state, $v'=1$. A similar behavior can be found between $v'=1$ and $v'=2$ at the $v'=2$ threshold. It would appear that on the XXZLG surface the next open product vibrational state is populated in preference to the other lower ones, pointing to nonstatistical dynamics. The same behavior can be observed for TU surface.

Figure 1 also clearly shows a difference in the threshold energies for all final vibrational energies between the XXZLG surface on the one hand and the other two surfaces on the other hand. The energy thresholds on the DMBE IV and the TU surfaces are similar while the ones on the XXZLG surface are shifted to significantly lower energies.

Figure 2 shows the product rotational distributions for the DMBE IV, XXZLG, and TU surfaces for the first two product vibrational states, $v'=0,1$. The distributions shown have been averaged over a small energy window due to the narrow structures in the reaction probabilities. The energy windows presented here have been chosen to coincide with different features of the reaction probabilities involved. Panel (a) shows the distributions for $v'=0$ for the DMBE IV surface. For energies below 1.2 eV most rotational states are similarly populated. Above this energy high rotational states are favored. This is especially visible for the distribution for the 1.4–1.45 eV energy window which features a large peak for $j'=13,14,15$. For $v'=1$ it is a similar picture, high rotational states are populated in preference to the low rotational states. This is quite possibly due to the onset of the proposed direct mechanism above 1.2 eV which may lead to nonstatistical behavior. The rotational distributions therefore present a mixture of both mechanisms for energies above 1.2 eV.

Panel (c), $v'=0$, shows that for the XXZLG surface for energies below 1.4 eV all rotational states which are open are populated. Above 1.4 eV the higher rotational states are favored. Interestingly this behavior is similar to the DMBE IV surface. However, for the XXZLG surface the magnitude

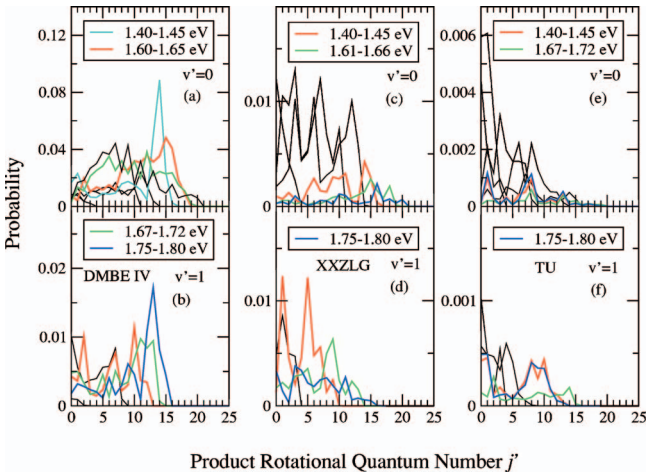

FIG. 2. (Color) Product rotational distributions for the DMBE IV, XXZLG, and TU surfaces calculated with the RWP1 method. Panel (a) Rotational distribution for the ground product vibrational state $v'=0$, DMBE IV. Panel (b) Distribution for $v'=1$, DMBE IV. Panel (c) Rotational distribution for the ground product vibrational state $v'=0$, XXZLG. Panel (d) Distribution for $v'=1$, XXZLG. Panel (e) Rotational distribution for the ground product vibrational state $v'=0$, TU. Panel (f) Distribution for $v'=1$, TU. The distributions are for O_2 reactant molecule initially in its ground state ($v=0$, $j=1$). The distributions shown are averaged for several small energy windows in the range from 0.8 to 1.8 eV. Distributions for energies below 1.4 eV are not distinguished but shown as black lines. Distributions for energies above 1.4 eV are shown in color to show the differences with energy and surface.

for $v'=0$ is so small for these energies that their contribution to the all over distributions is not noticeable. Panel (d) shows the rotational distribution for $v'=1$. Also here high rotational states are favored or at least equally populated to the low rotational states at high energies but the effect is not as pronounced as for $v'=0$.

Panels (e) and (f) show the product rotational distributions for the TU surface. The general picture here is different to the other two surfaces. For the TU surface the rotational distributions tend to peak at the lower rotational states for both vibrational product states. The distributions for energies above 1.4 eV for both states seem to be a mixture and show peaks at lower and high rotational states.

More detailed figures, Figs. 12, 13, and 14, for all rotational distributions can be found in the supplementary material.[55]

In an early experimental study Bronikowski *et al.*[7] reported rotational distributions for $v'=0$ and $v'=1$ for a collision energy of 1.6 eV which correspond to $\approx 1.69-1.7$ eV of total energy. Their experimental rotational distributions for $v'=0$ peak at $j'=15$ and the distribution for $v'=1$ peaks at $j'=10$. Our results for the DMBE IV surface, Fig. 2 panels (a) and (b), are in general agreement with the early experimental results. Our results also confirm the findings of the earlier calculations by Pack *et al.*[10] and Dai and Zhang[12] for the DMBE IV surface. The distributions for the DMBE IV surface peak at high rotational states for all energy ranges considered here. The rotational distributions from the XXZLG surface for energies above 1.6 eV are also in line with the experimental results. For energies above 1.6 eV the distributions are biased towards the higher rotational states which are favored over the lower ones. This picture is different for the TU surface. Here the distributions are biased towards the low rotational states, often peaking at $j'=0$. Low rotational states are favored for all energy ranges considered. Only for energies around 1.8 eV does this behavior seem to change.

The reason why the three surfaces yield such strikingly different reaction probabilities is unfortunately not easy to obtain from our calculations, but would rather require a detailed analysis of the surfaces themselves. Thus, we will just highlight a few differences, which may lead to the discrepancies between the surfaces. The XXZLG surface is based on a spline interpolation of high quality *ab initio* points covering O_1-O_2 distances from 1.4 to 12.5 a.u. and O_1-H distances from 1.0 to 11.0 a.u. This means the long-range potential is only described up to 11.0 a.u., which is a problem, since converged reaction probabilities require maximum values for scattering and vibrational coordinates of approximately 20 a.u. In addition, the potential is cut off at 0.135 a.u., which is well below the potential cutoffs used in both programs. However, rerunning RWP2 for DMBE IV with the lower cutoff values in the point selection scheme showed that this had an insignificant effect on the total reaction probabilities. As a result, this can be excluded as the cause of the discrepancy between the DMBE IV and XXZLG surfaces. On the other hand, the interaction/well region is described well by this potential, given previous calculations for the HO_2 complex.[29,56]

The TU surface was constructed on the basis of *ab initio* calculations for the $H+O_2$ and $HO+O$ dissociations. The representations for both two-dimensional potentials were combined by using a switching technique. The authors concede that "the global potential does not represent all ranges of the potential equally well by focusing on the minimum energy path potential."[2] The potential gives good agreement with experiment for the study of the kinetics for the $H+O_2$ reaction, although there are doubts about the accuracy of the interaction region. However, it is interesting to point out here that the TU and XXZLG surfaces do both give total reaction probabilities that are similar in their general features, despite the completely different way in which they were constructed.

Finally, the DMBE IV surface, which is the oldest of the three surfaces, gives a qualitatively different behavior for the total reaction probability. Meijer and Goldfield[15] attributed the rise in reaction probability above 1.2 eV to the onset of a direct mechanism. This rise in reaction probability seems to be absent for the XXZLG and the TU surfaces and could therefore be an artifact of the DMBE IV surface as suggested by Lin *et al.*

2. Initial state excitation

In this section we look at the effect of the excitation of the initial rotational and vibrational state on the reaction probabilities. Figure 3 shows the reaction probabilities for the DMBE IV, XXZLG, and TU surfaces for five different initial rotational states, $j=0,3,5,7,9$. Panel (a) of Fig. 3 shows that rotational excitation decreases reactivity for the DMBE IV surface especially for energies above 1.2 eV. The effect is largest in going from $j=1$ to $j=3$. Subsequent rotational excitation has an effect on the reaction probability as well albeit to a lesser degree. Our reaction probabilities for

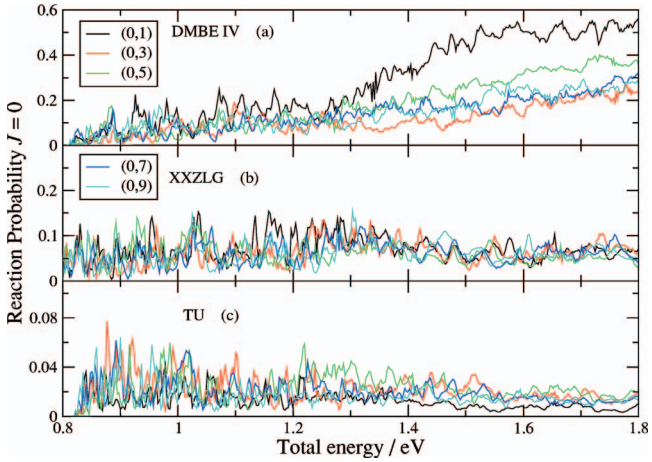

FIG. 3. (Color) Reaction probabilities vs total energy in eV by the RWP1 method on the (a) DMBE IV, (b) XXZLG, and (c) TU surfaces for different rotational excited initial states, $j=0$ (black line), $j=3$ (red line), $j=5$ (green line), $j=7$ (blue line), and $j=9$ (cyan line).

$j=3$ in the range from 0.8 to 1.3 eV confirm the results by Lin *et al.*[38] where a slight decrease in magnitude was noticeable. Figure 3(b) shows the reaction probabilities for the XXZLG surface. For this surface the initial rotational state excitation has no significant effect on the magnitude of the reaction probability. These findings seem to be in line with the ones by Lin *et al.*[38] where it seems that for $j=3$ the probability is only slightly decreased. Figure 3(c) shows the probabilities for the TU surface. For this surface one can see a noticeable increase in reactivity especially for energies above 1.25 eV. The vibrational product state resolved reaction probabilities (figures available in the supplementary information[55]) show that the decrease for the DMBE IV surface is mainly due to its effect on the ground vibrational product state probability. For the XXZLG surface there is no significant effect for the different vibrational product states. For the TU surface the effect can be seen for all vibrational product state probabilities.

Figure 4 shows the reaction probabilities for the DMBE IV, XXZLG, and TU surfaces for three different initial vibrational states, $v=0,1,2$. Panel (a) of Fig. 4 shows the reaction probabilities for the DMBE IV surface. Like in the case of the excited initial rotational states the reactivity is decreased. This is consistent with the results from Ref. 9 where the authors also found that initial vibrational state excitation decreases the reaction probability. For the XXZLG surface, panel (b), there is a noticeable increase in magnitude when going from the ground vibrational initial state to the first two excited states. This increase is noticeable especially for energies above 1.25 eV. The findings here for the (1,1) initial state for the DMBE IV and XXZLG surface in the energy range from 0.8 to 1.3 eV are similar to those reported in Ref. 38. The effects observed in the present study are mainly visible for energies above 1.3 eV. Panel (c) shows the same probabilities for the TU surface and one can see a significant increase for the excited initial vibrational state probabilities over the whole energy range shown. Again, for the DMBE IV surface the decrease is mainly due to a decrease in the $v'=0$ probability, see supplementary material in Ref. 55. For the XXZLG surface the increase is noticeable for all product states which is also the case for the TU surface.

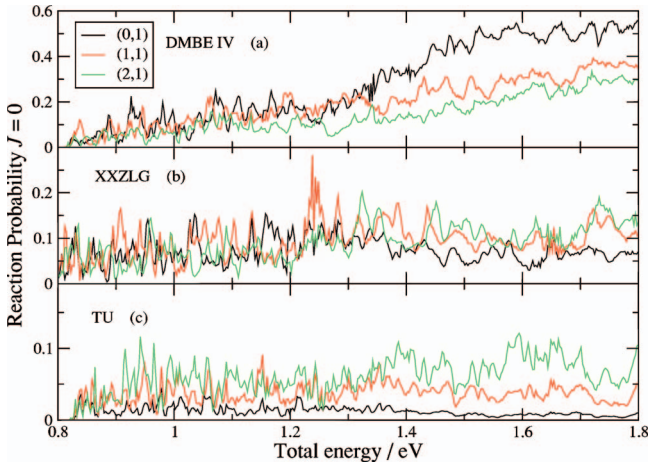

FIG. 4. (Color) Reaction probabilities vs total energy in eV by the RWP1 method on the (a) DMBE IV (b) XXZLG, and (c) TU surfaces for different vibrational excited initial states, $v=0$ (black line), $v=1$ (red line), and $v=2$ (green line).

Sultanov and Balakrishnan[22] calculated cumulative reaction probabilities (CRP) for $J=0$ on the DMBE IV and TU surfaces. They report that the CRP on the TU surface are 10%–50% higher than the CRP on the DMBE IV surface for energies above 0.9 eV. If we consider our results from Figs. 10, 11, and 1 alone this result is a surprise as the total reaction probabilities from the TU surface are so much smaller than those from the DMBE IV surface. Figures 3 and 4 offer an explanation for the results from Ref. 22 as the probabilities for the TU surface show a significant increase with initial state excitation while the probabilities for the DMBE IV surface show a significant decrease.

B. $J>0$ total reaction probabilities

In this section we will now investigate the influence of the initial rotational state excitation on the total reaction probabilities when the total angular momentum J is not equal to zero. We will present results for $J=2,4$ and $j=1,3,5$ for the DMBE IV and the XXZLG surfaces.

Figure 5 shows the total reaction probabilities for $J=2$ for the DMBE IV and the XXZLG surfaces from the reactant ground state. The averaged $J=2$ probability [see Eq. (1)] and the contributing probabilities for each initial Ω state are shown. For the DMBE IV surface the $J=2$ probability is significantly smaller than the probability for $J=0$. The probability for $\Omega=0^+$ (i.e., the initial projection quantum number equals 1 with even spectroscopic parity) is the largest while the probabilities for $\Omega=1^+$ and $\Omega=1^-$ (the only odd parity initial state) are very similar. For the XXZLG surface the general picture is similar. The probability is decreased for $J=2$, compared to $J=0$ but the effect is not as pronounced as for the DMBE IV surface. And also here the $\Omega=0^+$ probability is largest while the other two probabilities are similar in magnitude.

Figure 6 shows the total reaction probability for $J=4$ for the DMBE IV and XXZLG surfaces again for $O_2(0,1)$. The average over all contributing values of Ω is shown as well as

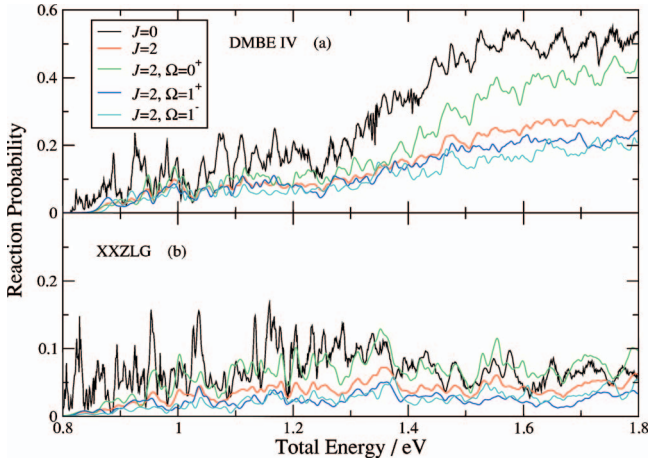

FIG. 5. (Color) Reaction probabilities for $J=0$ (black line) and $J=2$ for the DMBE IV and the XXZLG surfaces calculated with the RWP2 method. For $J=2$ the three Ω contributions are shown ($\Omega=0^+$, green line; $\Omega=1^+$, blue line; and $\Omega=1^-$, cyan line) as well as the total $J=2$ (red line) probability (averaged over all Ω).

all individual Ω probabilities. Comparing the total reaction probability for both surfaces to the $J=0$ and $J=2$ probabilities in the previous figure it is clear to see that the probability is decreased for both surfaces. The decrease is not as pronounced for the XXZLG surface as for the DMBE IV surface. The latter has already been reported on by Meijer and Goldfield.[15–19] For both surfaces the $\Omega=0^+$ probability is the largest while the $\Omega=1^{\pm}$ are the smallest and of similar magnitude. It turns out to be a general observation that both parity states will give similar reaction probabilities for a given value of Ω.

From now on we will only show the overall reaction probabilities for each value for J. Individual Ω probabilities are available as supplementary information in Ref. 55, Figs. 21–24. In these figures the odd parity probabilities have been omitted as they are always very similar to the even parity probabilities.

Figure 7 shows the reaction probabilities for the DMBE IV surface for $J=2$ and $J=4$ for three different initial rotational states, $j=1,3,5$. Panel (a) shows the averaged (over all contributing initial Ω) probabilities for $J=2$ and panel (b) shows the probabilities for $J=4$. For $J=2$ the probability increases for initial rotational excitation $j=3$. This is clearly different to the $J=0$ probability where the magnitude was significantly decreased for this initial rotational state, see Fig. 3. The probability for $j=5$ is similar to the $j=1$ probability. Figure 7(b) shows that for $J=4$ the $j=1$ and $j=3$ initial states result in similar reaction probabilities, while $j=5$ gives a significantly larger reaction probability.

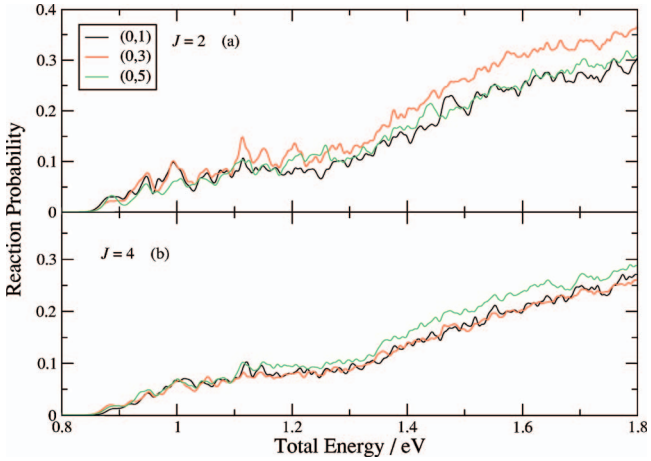

FIG. 7. (Color) Reaction probabilities for the DMBE IV surface for different initial rotational states, $j=1$ (black line), $j=3$ (red line), and $j=5$ (green line). Panel (a) Probabilities for $J=2$. Panel (b) Probabilities for $J=4$.

Figure 8 shows the reaction probabilities for the XXZLG surface for $J=2$ (a) and $J=4$ (b) for three different initial rotational states, $j=1,3,5$. Here, the situation is not as clear as for the DMBE IV surface and in fact would appear to be almost independent of initial rotational angular momentum.

Analyzing the individual Ω calculations for $J=2$ and $J=4$ for both surfaces, we also see contrasting behavior (for figures see supplementary information in Ref. 55). In particular, we can see that for the XXZLG surface the highest values of Ω give probabilities which are always the smallest in magnitude. In fact the magnitude decreases with increas-

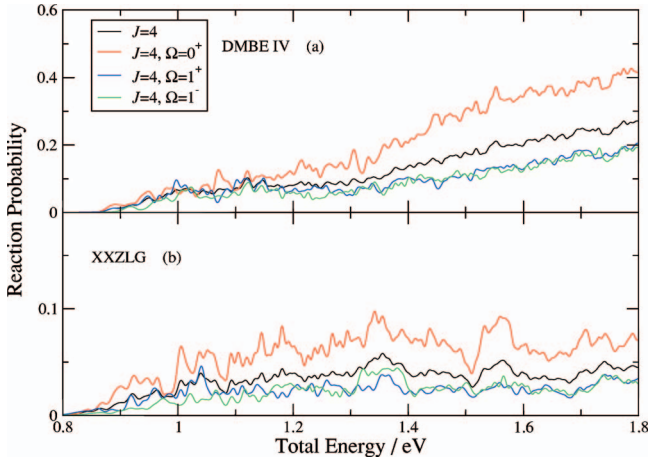

FIG. 6. (Color) Reaction probabilities for $J=4$ (black line) for the DMBE IV and the XXZLG surfaces calculated with the RWP2 method. The three Ω contributions are shown ($\Omega=0^+$, red line; $\Omega=1^+$, blue line; and $\Omega=1^-$, green line).

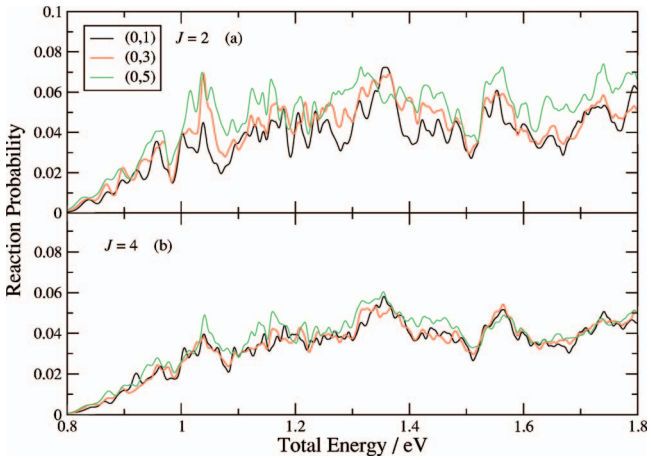

FIG. 8. (Color) Reaction probabilities for the XXZLG surface for different initial rotational states, $j=1$ (black line), $j=3$ (red line), and $j=5$ (green line). Panel (a) Probabilities for $J=2$. Panel (b) Probabilities for $J=4$.

ing value of Ω. For the DMBE IV surface the picture is very different. In several cases probabilities for higher values of Ω are higher in magnitude than the one for $\Omega=0^+$. Also in some cases the highest Ω value has the largest probability.

The above observations can be rationalized in the following way. For the terms diagonal in the Ω quantum number, changing initial total or rotational angular momentum will only change the following term in the Hamiltonian:[15]

$$T^{cf} = \frac{J(J+1) + j(j+1) - 2\Omega^2}{2\mu R^2}. \tag{2}$$

For $J=0$ one would expect initial rotational excitation to give a centrifugal barrier in the entrance channel, provided that the initial rotational excitation stays conserved long enough for the barrier to be important. This is apparently the case for the DMBE IV potential, but not for the XXZLG potential nor for the TU potential (see Sec. III A 2). For $J>0$ this effect will be even more pronounced for low Ω initial states. However, for high initial Ω states the barrier will disappear. The result would be an enhancement of the reaction probability compared to the low values for Ω. This is precisely what is found for the DMBE IV surface, leading us to conclude that Ω is a better quantum number in that case than for the XXZLG surface, where Ω apparently scrambles completely very quickly (through Coriolis coupling), resulting in a similar reaction probability for all initial Ω states. As an aside we want to point out that the centrifugal barrier in Eq. (2) will also mean that if we extend these calculations to larger J, we have to move the starting point of the wavepacket further into the reactants channel, so that the overall potential there will be as small as possible.

In Ref. 19 the authors assumed that the calculation of cross section based only on calculations for $j=1$ will lead to a cross section which is an upper bound to the real cross section. This argument was based on the excited initial state results by Zhang and Zhang.[9] The observations indicated above would contradict this assumption. To investigate this somewhat further we plotted the weighted sum over J of the reaction probabilities based on the calculations so far for each of the initial rotational states and the two surfaces in Fig. 9. These weighted sums, $P_{vj}(E)$, are obtained via the following equation:

$$P_{vj}(E) = \sum (2J+1) P^J_{vj}(E). \tag{3}$$

These are used in the calculation of total cross sections as

$$\sigma_{(v,j)}(E_{tr}) = \frac{1}{3}\frac{\pi}{k^2_{vj}} \sum_J (2J+1) P^J_{vj}(E_{tr}), \tag{4}$$

where $k_{vj}=\sqrt{2\mu(E-E_{vj})}$ is the relative momentum of the incoming particle and E_{vj} is the energy of the initial rovibrational state of O_2.

As can be seen from Fig. 9 it is not immediately obvious that a cross section obtained for $j=1$ will give an upper bound to the "real" cross section. Both for the DMBE IV surface and the XXZLG surface it is the $j=5$ sum which appears to be largest, although the difference with $j=1$ and $j=3$ is small. Moreover, the cross section is expressed in terms of the translational energy. This means that for a similar total energy the translational energy for $j=5$ (and therefore its momentum) will be lower than for the $j=1$ state. This means that even if the weighted reaction probabilities are similar, the resulting cross sections for $j=5$ will be larger than for $j=1$. In turn this will lead to larger overall cross sections if one Boltzmann averages the cross sections for all initial states. This would potentially lead to closer agreement with the experimental cross sections.

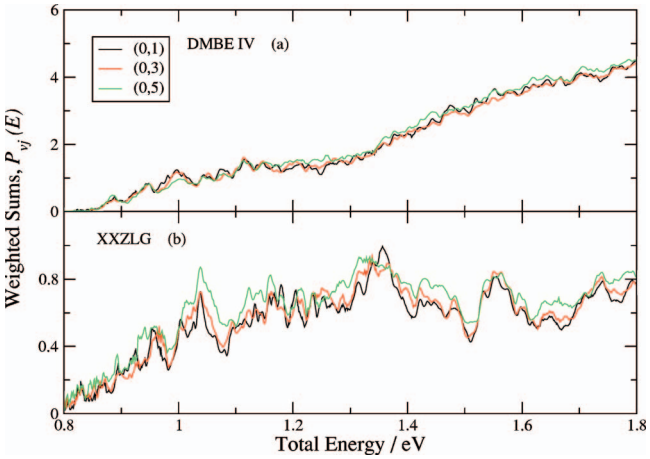

FIG. 9. (Color) Weighted sum [see Eq. (3)] over the three total angular momenta $J=0$, 2, 4 for the initial rotational states $j=1$ (black line), $j=3$ (red line), and $j=5$ (green line) for the (a) DMBE IV and the (b) XXZLG surfaces.

IV. CONCLUSIONS

We reported total and state-to-state reaction probabilities calculated employing two different time-dependent wavepacket computer programs, for three different potential energy surfaces. Our calculated initial excited state reaction probabilities for $J=0,2,4$ for the XXZLG surface [except for $J=0$, $(v,j)=(0,3)$, and $(1,1)$] and for the DMBE IV surface (except for $J=0$) in the range from 0.8 to 1.8 eV are the first to be reported to date.

The total reaction probability obtained on the DMBE IV surface shows a sudden increase above 1.2 eV. Our results for the DMBE IV surface are in excellent agreement with the results from earlier calculations performed employing this surface. In contrast the total reaction probabilities obtained employing the TU and XXZLG surfaces do not feature this increase above 1.2 eV but in fact show a decrease in magnitude with increasing energy. The total probabilities from those two surfaces show similar resonance structures as the probability obtained from the DMBE IV surface. They are narrow below 1.2 eV and broader above this energy. Our results for the DMBE IV and XXZLG surfaces confirm the findings of the first study which included those both surfaces.

The state-to-state reaction probabilities show that the differences between the DMBE IV and the XXZLG are mainly due to the $v'=0$ probability. The probabilities for the $v'=1$ and $v'=2$ product vibrational states agree much better. The increase in the total reaction probability for the DMBE IV surface above 1.2 eV is due to the increase in magnitude of the $v'=0$ state probability. The decrease in the total reaction probability for the XXZLG above 1.2 eV is due to the

rapid decrease in magnitude of the $v'=0$ state probability. Compared to the probabilities from the DMBE IV and the XXZLG surfaces the probability from the TU surface is very small. It shows similar behavior to the XXZLG surface, displaying the same decrease for energies above 1.2 eV and which again is due to the rapid decrease in magnitude of the $v'=0$ state probability.

We presented rotational product state distributions for all three surfaces. The rotational distributions for the DMBE IV surface are peaked at high rotational states for energies above 1.2 eV for $v'=0$ and for energies above 1.6 eV for $v'=1$. The rotational distributions for $v'=0$ on the XXZLG surface are also peaked at high rotational states for energies above 1.4 eV. The rotational distributions for the TU surface are peaked at the lower rotational states showing different behavior to the other two surfaces.

The excited initial rotational and vibrational state probabilities for $J=0$ obtained on the DMBE IV surface show a significant decrease in magnitude in all cases considered here. The probabilities obtained on the XXZLG and the TU surfaces on the other hand show an increase in magnitude. Again the TU and the XXZLG show similar general behavior.

We also presented reaction probabilities for $J>0$ for the DMBE IV and the XXZLG surfaces. To the best of our knowledge the individual probabilities for $J=2$ and $J=4$ are the first to be reported for XXZLG surface. The reaction probabilities for the DMBE IV and the XXZLG surfaces for total angular momentum $J=2$ and $J=4$ are smaller in magnitude than the $J=0$ probabilities.

We carried out calculations for two excited rotational states for the DMBE IV and the XXZLG surfaces for $J=2$ and $J=4$ to extend our investigation of the effects of the initial rotational excitation on the dynamics. For the DMBE IV surface the rotational excitation significantly decreased the reaction probability for $J=0$. In the case of nonzero total angular momentum the reactivity is increased. For XXZLG surface the reactivity was not affected by the initial rotational excitation for any value of total angular momentum we looked at.

We present here reaction probabilities for $J=0$, 2, and 4 only and it remains to be seen how reaction cross sections or rate constants will be affected when the TU or the XXZLG surface is employed. It is important to note here that this will require a rigorous treatment of Coriolis coupling for this system. Approximation methods such as J-shifting or helicity decoupling to obtain reaction cross section have shown to be flawed.[18] It will therefore require full quantum dynamical calculations to see if the TU or the XXZLG surface gives significantly different results from the DMBE IV surface. However, based on the current calculations, we expect this to be the case. Therefore, we have to conclude that the three surfaces are giving quantitatively different cross sections. Consequently, we feel that the potential for the $H+O_2$ reaction can still be improved further to get better agreement with the available experimental data. Hereby, we expect that nonadiabatic effects, both in the O+OH exit channel and for the HO_2 intermediate, will most likely need to be considered as well.

Recently some of the authors of the XXZLG surface published a new analytical form of the XXZLG surface.[37] They present two new surfaces obtained by fitting the *ab initio* data using the reproducing kernel Hilbert space method. Their RKHS-v is intended for calculations of the HO_2 vibrational spectrum and the RKHS-r surface offers a global surface for reaction dynamics. These two new surfaces have been improved to the original spline fitted XXZLG surface. Around 280 points in higher energy regions have been corrected and the new potentials are accurate up to 12 eV from the potential minimum compared to 6 eV for the XXZLG surface. The announced calculations for $J>0$ will hopefully shed some light as to the effect of the XXZLG surface on the reaction cross sections of the $H+O_2$ reaction.

Note added in proof. During the publication process of this manuscript a new study by Honvault *et al.*[57] was brought to our attention where the authors report differential cross section for a few selected low energies and several initial rovibrational states employing the XXZLG surface. All partial waves up to total angular momentum $J=32$ have been included in this new study employing a time-independent method. The authors also report integral cross section for the XXZLG surface for energies up to 1.0 eV and the behavior is similar to the one of the DMBE IV results in this energy range. The integral cross sections have been obtained using a time-dependent method including all total angular momenta up to $J=50$. The announced calculations for higher values of J and the extension of the results to higher energies by the authors will certainly answer many of the questions raised with regards to the differences between the DMBE IV and XXZLG surfaces and the effect of the XXZLG surface on the cross sections for energies above 1.25 eV.

ACKNOWLEDGMENTS

The RWP1 calculations reported in this paper have been performed on the CMS computational facility housed by the Centre for Computational Molecular Science, Australian Institute for Bioengineering and Nanotechnology, University of Queensland, Australia. These computational facilities have been purchased from funds provided by the University of Queensland and the Queensland Smart State Research Facilities Fund. The RWP2 calculations have been performed at the Theoretical Chemistry Group at the University of Sheffield and on computers part of the White Rose Grid in Leeds and Sheffield. One of the authors (M.H.) would like to thank Sun Microsystems for funding. The authors would like to thank Russ Pack and John Zhang for sending them their results. They are also grateful to Daiqian Xie for sending them the XXZLG surface. They would also like to thank Antonio Varandas for sending them the DMBE IV surface. The authors are grateful to Jürgen Troe for sending them the codes for the TU surface and for helpful comments. The authors would also like to thank Evelyn Goldfield for helpful comments.

[1] W. C. Gardiner, *Combustion Chemistry* (Springer, Berlin Germany, 1984).
[2] J. Troe and V. G. Ushakov, J. Chem. Phys. **115**, 3621 (2001).
[3] R. J. Duchovic and M. A. Parker, J. Phys. Chem. A **109**, 5883 (2005).

[4] S. M. Hwang, S.-O. Ryu, K. J. De Witt, and M. J. Rabinowitz, Chem. Phys. Lett. **408**, 107 (2005).
[5] C. Xu, D. Xie, D. H. Zhang, S. Y. Lin, and H. Guo, J. Chem. Phys. **122**, 244305 (2005).
[6] S. Y. Lin, E. J. Rackham, and H. Guo, J. Phys. Chem. A **110**, 1534 (2006).
[7] M. J. Bronikowski, R. Zhang, D. J. Rakestraw, and R. N. Zare, Chem. Phys. Lett. **156**, 7 (1989).
[8] R. T Pack, E. A. Butcher, and G. A. Parker, J. Chem. Phys. **99**, 9310 (1993).
[9] D. H. Zhang and J. Z. H. Zhang, J. Chem. Phys. **101**, 3671 (1994).
[10] R. T Pack, E. A. Butcher, and G. A. Parker, J. Chem. Phys. **102**, 5998 (1995).
[11] B. Kendrick and R. T Pack, J. Chem. Phys. **104**, 7502 (1996).
[12] J. Dai and J. Z. H. Zhang, J. Phys. Chem. **100**, 6898 (1996).
[13] R. Fei, X. S. Zheng, and G. E. Hall, J. Phys. Chem. A **101**, 2541 (1997).
[14] B. Kendrick and R. T Pack, J. Chem. Phys. **106**, 3519 (1997).
[15] A. J. H. M. Meijer and E. M. Goldfield, J. Chem. Phys. **108**, 5404 (1998).
[16] A. J. H. M. Meijer and E. M. Goldfield, J. Chem. Phys. **110**, 870 (1999).
[17] E. M. Goldfield and A. J. H. M. Meijer, J. Chem. Phys. **113**, 11055 (2000).
[18] A. J. H. M. Meijer and E. M. Goldfield, Phys. Chem. Chem. Phys. **3**, 2811 (2001).
[19] M. Abu Bajeh, E. M. Goldfield, A. Hanf, C. Kappel, A. J. H. M. Meijer, H.-R. Volpp, and J. Wolfrum, J. Phys. Chem. A **105**, 3359 (2001).
[20] H. Zhang and S. C. Smith, J. Chem. Phys. **117**, 5174 (2002).
[21] H. Zhang and S. C. Smith, J. Chem. Phys. **116**, 2354 (2002).
[22] R. A. Sultanov and N. Balakrishnan, J. Phys. Chem. A **108**, 8759 (2004).
[23] T. González-Lezana, E. J. Rackham, and D. E. Manolopoulos, J. Chem. Phys. **120**, 2247 (2004).
[24] P. Bargueño, T. González-Lezana, P. Larrégaray, L. Bonnet, and J. C. Rayez, Phys. Chem. Chem. Phys. **9**, 1127 (2007).
[25] L. B. Harding, J. Troe, and V. G. Ushakov, Phys. Chem. Chem. Phys. **2**, 631 (2000).
[26] J. M. C. Marques and A. J. C. Varandas, Phys. Chem. Chem. Phys. **3**, 505 (2001).
[27] L. B. Harding, J. Troe, and V. G. Ushakov, Phys. Chem. Chem. Phys. **3**, 2630 (2001).
[28] J. M. C. Marques and A. J. C. Varandas, Phys. Chem. Chem. Phys. **3**, 2632 (2001).
[29] H. Zhang and S. C. Smith, Phys. Chem. Chem. Phys. **3**, 2282 (2001).
[30] H. Zhang and S. C. Smith, J. Chem. Phys. **20**, 9583 (2004).
[31] H. Zhang and S. C. Smith, Phys. Chem. Chem. Phys. **6**, 884 (2004).
[32] S. Y. Lin, D. Xie, and H. Guo, J. Chem. Phys. **125**, 091103 (2006).
[33] X. Wu and E. F. Hayes, J. Chem. Phys. **107**, 2705 (1997).
[34] M. R. Pastrana, L. A. M. Quintales, J. Bradão, and A. J. C. Varandas, J. Phys. Chem. **94**, 8073 (1990).
[35] B. Kendrick and R. T Pack, J. Chem. Phys. **102**, 1994 (1995).
[36] C. F. Melius and R. J. Blint, Chem. Phys. Lett. **64**, 183 (1979).
[37] D. Xie, C. Xu, T.-S. Ho, H. Rabitz, G. Lendvay, S. Y. Lin, and H. Guo, J. Chem. Phys. **126**, 074315 (2007).
[38] S. Y. Lin, H. Guo, P. Honvault, and D. Xie, J. Phys. Chem. B **110**, 23641 (2006).
[39] D. Skouteris, J. F. Castillo, and D. E. Manolopoulos, Comput. Phys. Commun. **133**, 128 (2000).
[40] S. K. Gray and G. G. Balint-Kurti, J. Chem. Phys. **108**, 950 (1998).
[41] M. Hankel, G. G. Balint-Kurti, and S. K. Gray, J. Chem. Phys. **113**, 9658 (2000).
[42] M. Hankel, G. G. Balint-Kurti, and S. K. Gray, J. Phys. Chem. **105**, 2330 (2001).
[43] G. G. Balint-Kurti, R. N. Dixon, and C. C. Marston, J. Chem. Soc., Faraday Trans. **86**, 1741 (1990).
[44] G. C. Groenenboom and D. T. Colbert, J. Chem. Phys. **99**, 9681 (1993).
[45] S. C. Althorpe, J. Chem. Phys. **114**, 1601 (2001).
[46] K. Yuan, Y. Cheng, X. Liu, S. Harich, X. Yang, and D. H. Zhang, Phys. Rev. Lett. **96**, 103202 (2006).
[47] S. Y. Lin and H. Guo, Phys. Rev. A **74**, 022703 (2006).
[48] M. Hankel, S. C. Smith, R. J. Allan, S. K. Gray, and G. G. Balint-Kurti, J. Chem. Phys. **125**, 164303 (2006).
[49] Á. Vibók and G. G. Balint-Kurti, J. Chem. Phys. **96**, 7615 (1992).
[50] Á. Vibók and G. G. Balint-Kurti, J. Phys. Chem. **96**, 8712 (1992).
[51] E. M. Goldfield and S. K. Gray, Comput. Phys. Commun. **84**, 1 (1996).
[52] J. M. Brown, J. T. Hougen, K.-P. Huber, J. W. C. Johns, I. Kopp, H. Lefebvre-Brion, A. J. Merer, D. A. Ramsay, J. Rostas, and R. N. Zare, J. Mol. Spectrosc. **55**, 500 (1975).
[53] J. Tennyson and B. T. Sutcliffe, J. Mol. Spectrosc. **101**, 71 (1983).
[54] J. Tennyson and B. T. Sutcliffe, J. Chem. Phys. **77**, 4061 (1982).
[55] See EPAPS Document No. E-JCPSA6-127-024730 for Figs. 10–24. This document can be reached through a direct link in the online article's HTML reference section or via the EPAPS homepage (http://www.aip.org/pubservs/epaps.html).
[56] H. Zhang and S. C. Smith (unpublished).
[57] P. Honvault, S. Y. Lin, D. Xie, and H. Guo, J. Phys. Chem. A **111**, 5349 (2007).